Structure, Volume *34*

Supplemental Information

A correlative workflow for synaptic imaging by cryo-electron tomography

Thanh Thao Do, Anna Siegert, Florelle Domart, Fabienne Hahn, Christina Zeising, Sarah Muth, Constantin Pape, Kathrin Kusch, Thomas Dresbach, Silvio O. Rizzoli, Arsen Petrovic, and Rubén Fernández-Busnadiego

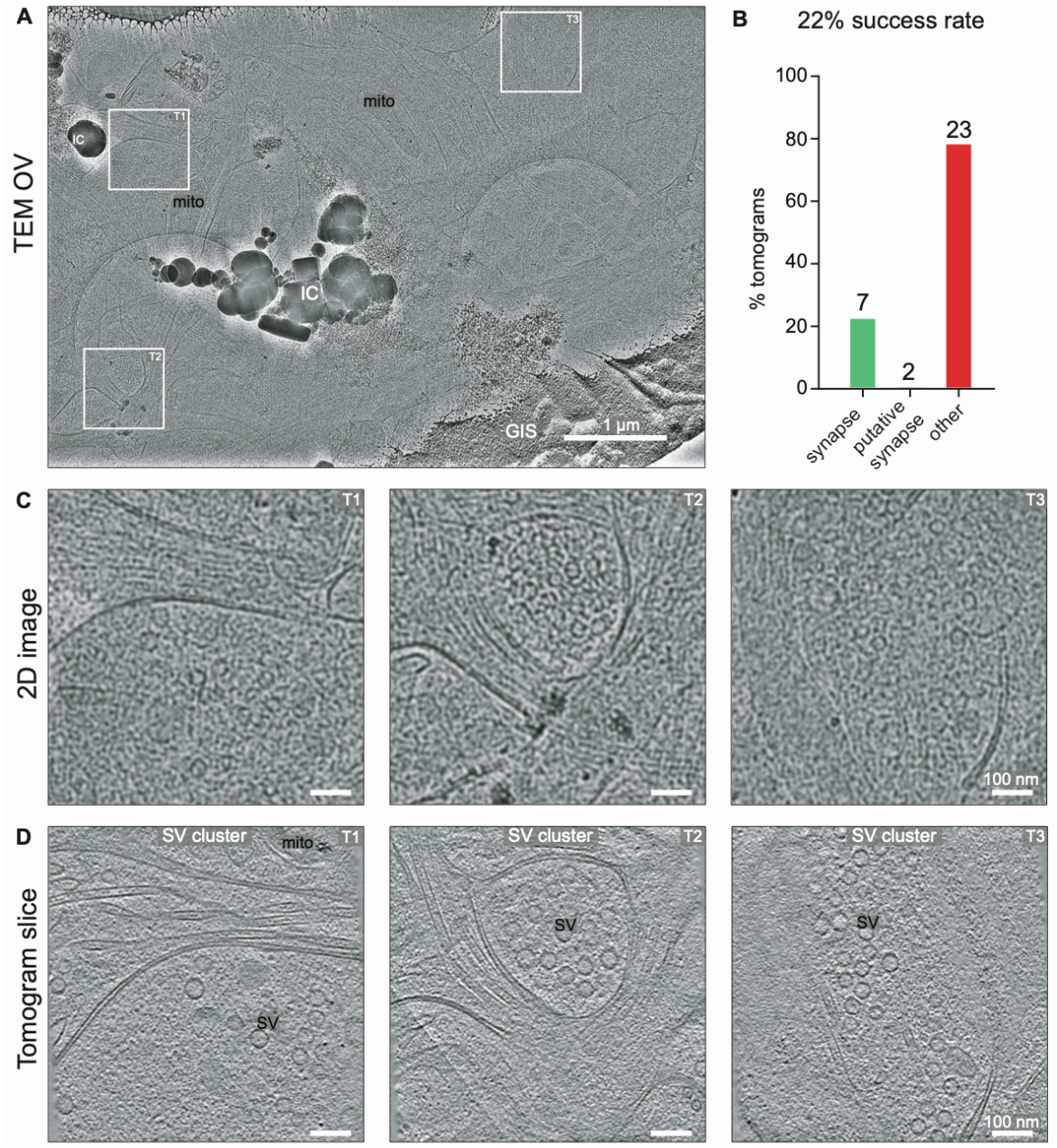

Figure S1. Synapse identification on unlabeled neurons, related to Figure 1.
(A) Cryo-TEM (TEM OV) low magnification (8700x) overview, showing a complex network of neuronal processes. GIS: platinum layer deposited by the gas injection system; IC: superficial ice crystal contamination. (B) Bar chart representing the success rate of synapse identification in tomograms. Success rate was defined as 100x the number of synaptic tomograms divided by the total number of tomograms recorded at fluorescent puncta. The number of tomograms per category is indicated on top of the respective bars. The categories were defined as follows: “synapse” refers to tomograms with clear synaptic contacts, containing a presynaptic terminal with SVs tethered at the AZ, and a postsynaptic partner separated by a well-defined synaptic cleft; “putative synapse” indicates cases where the synaptic contact was not as clear, e.g. due to missing wedge artifacts; “others” refers to non-synaptic areas. (C) Magnified views of regions indicated in A showing putative synaptic locations where tomograms were collected. (D) Slices of tomograms recorded at regions shown in C, containing SV clusters but no actual synapses. mito: mitochondrion; SV: SV cluster.

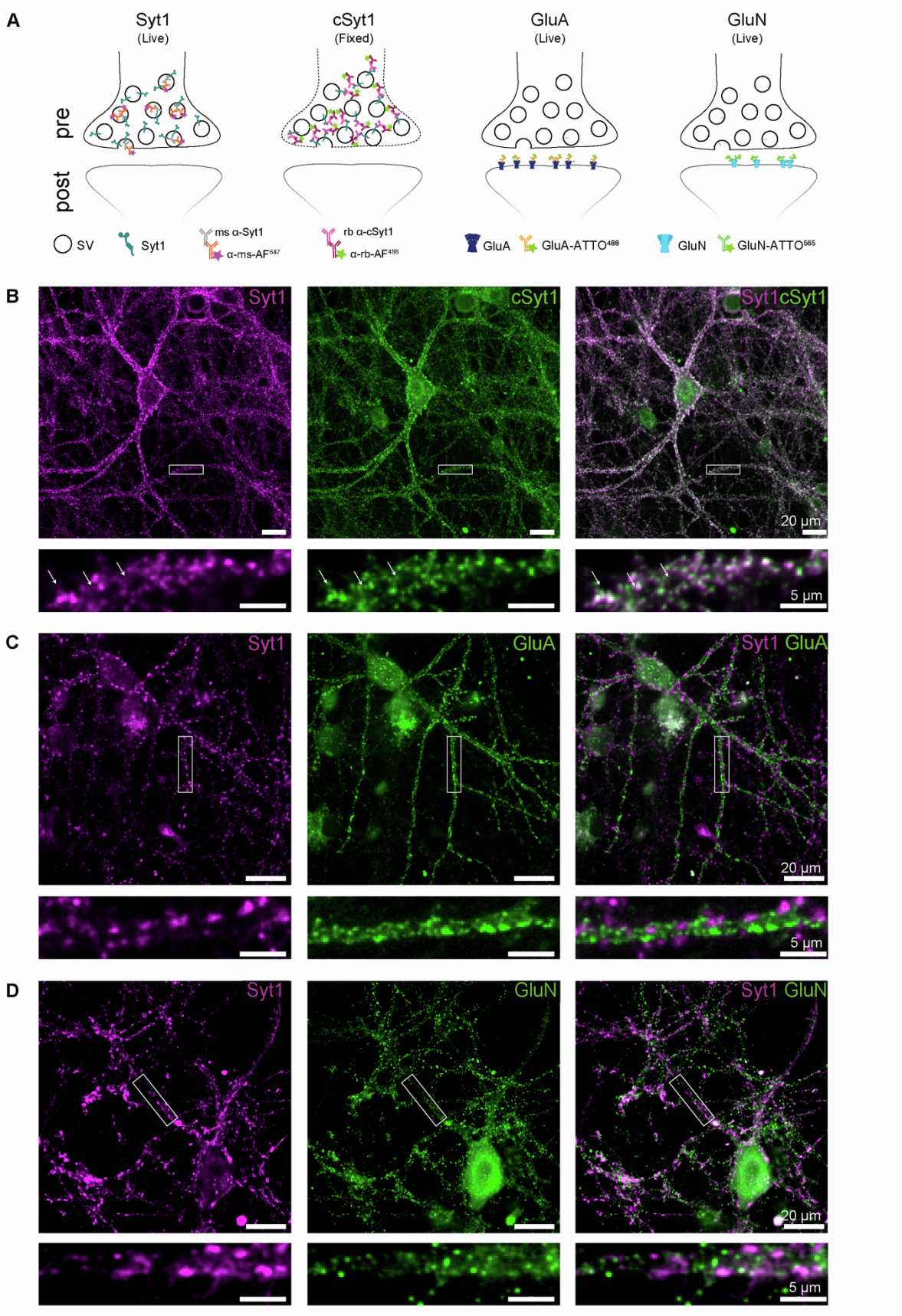
A
Syt1
(Live)
cSyt1
(Fixed)
GluA
(Live)
GluN
(Live)
pre
post
SV
Syt1
ms α-Syt1
α-ms-AF547
rb α-cSyt1
α-rb-AF488
GluA
GluA-ATTO488
GluN
GluN-ATTO565
B
Syt1
cSyt1
Syt1cSyt1
20 µm
5 µm
C
Syt1
GluA
Syt1 GluA
20 µm
5 µm
D
Syt1
GluN
Syt1 GluN
20 µm
5 µm

Figure S2. Room temperature imaging upon live immunolabelling of pre- and postsynaptic terminals, related to Figure 1.

(A) Cartoons depicting the fluorescent labelling strategies used in B-D. Syt1 antibodies bind to the luminal domain of Syt1 extracellularly exposed upon exocytosis, thereby labelling recycling SVs, whereas cSyt1 antibodies bind the cytosolic part of Syt1 and therefore labels all SVs. While Syt1 antibodies can be used live, cSyt1 require fixation and permeabilization. Primary antibodies were either used in combination with a fluorescently labelled secondary antibody (B, “Syt1”, magenta and “cSyt1”, green) or directly conjugated to a fluorophore (C, D). GluA antibodies bind to extracellular epitopes of the GluA subunits of postsynaptic AMPA receptors. GluN antibodies bind to extracellular epitopes of GluN subunits of postsynaptic NMDA receptors. pre: presynaptic terminal; post: postsynaptic terminal.

(B) Live immunostaining of Syt1 to label recycling presynaptic terminals. Neurons were live labelled with a mouse monoclonal antibody against the luminal domain of Syt1 (“Syt1”). After fixation and permeabilization, neurons were labelled with a mouse monoclonal antibody against the cytosolic domain of Syt1 (“cSyt1”). White arrows point to cSyt1 puncta that do not co-localize with Syt1 puncta. (C) Live immunostaining of Syt1 and GluA receptors to label synapses. Neurons were live labelled with Syt1-ATTO647N (magenta) and GluA-ATTO488 (green). (D) Live immunostaining of Syt1 and GluN receptors to label synapses. Neurons were live labelled with Syt1-ATTO647N (magenta) and GluN-ATTO565 (green). Insets in B-D show a magnified view of the neuronal process indicated in the boxed region.

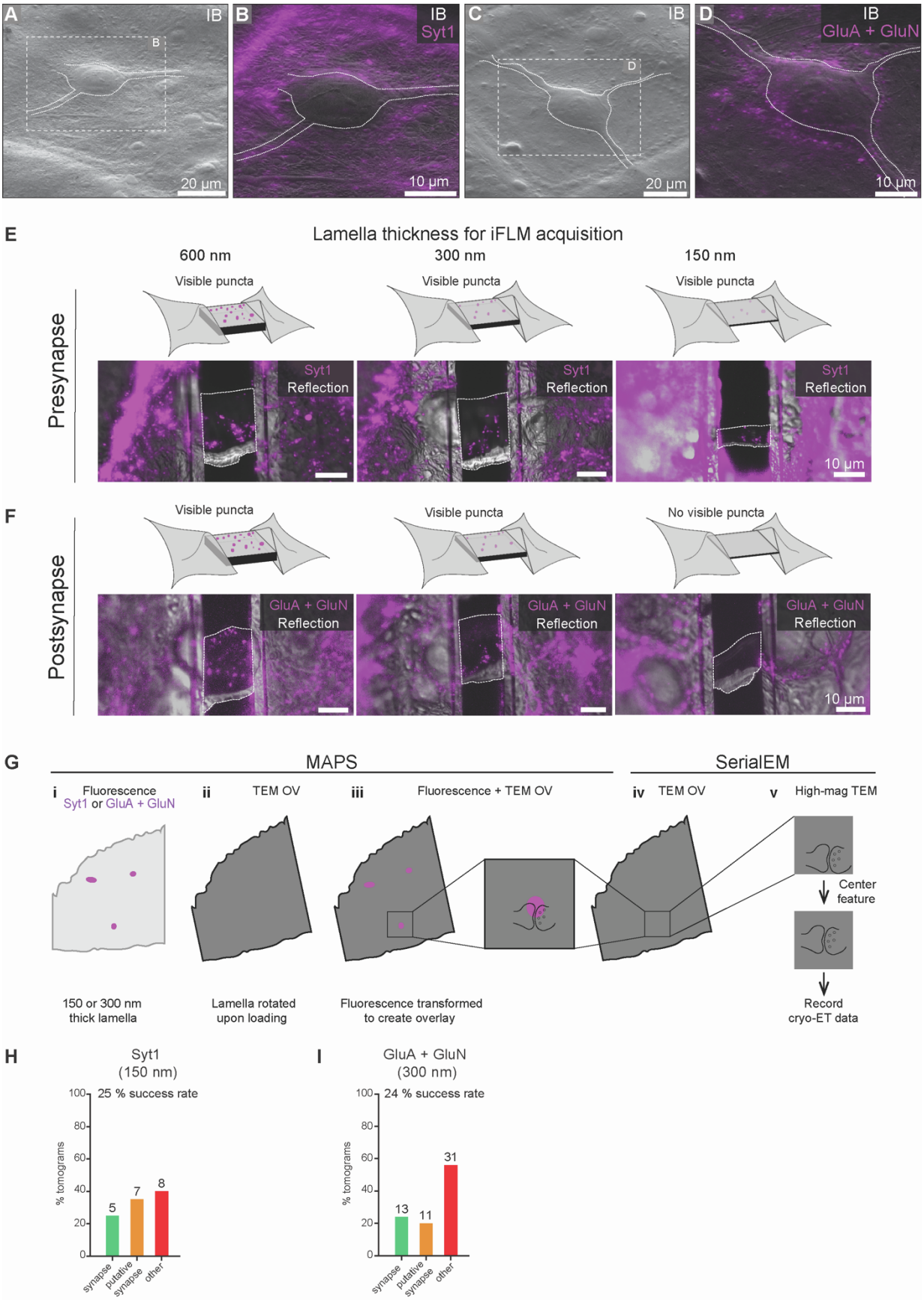
A
IB
B
20 µm
B
IB
Syt1
10 µm
C
IB
D
20 µm
D
IB
GluA + GluN
10 µm
E
Lamella thickness for iFLM acquisition
600 nm
300 nm
150 nm
Visible puncta
Visible puncta
Visible puncta
Presynapse
Syt1
Reflection
Syt1
Reflection
Syt1
Reflection
10 µm
F
Visible puncta
Visible puncta
No visible puncta
Postsynapse
GluA + GluN
Reflection
GluA + GluN
Reflection
GluA + GluN
Reflection
10 µm
G
MAPS
SerialEM
i Fluorescence
Syt1 or GluA + GluN
ii TEM OV
iii Fluorescence + TEM OV
iv TEM OV
v High-mag TEM
Center
feature
150 or 300 nm
thick lamella
Lamella rotated
upon loading
Fluorescence transformed
to create overlay
Record
cryo-ET data
H
Syt1
(150 nm)
25 % success rate
% tomograms
100
80
60
40
20
0
5
7
8
synapse
putative
synapse
other
I
GluA + GluN
(300 nm)
24 % success rate
% tomograms
100
80
60
40
20
0
13
11
31
synapse
putative
synapse
other

Figure S3. Cryo-FIB milling and cryo-CLEM workflow for live single-color synapse targeting, related to Figure 1.

(A-D) Identification of synapse-rich regions surrounding the cell body. (A and B) Labelling of presynaptic terminals using Syt1 luminal domain antibodies (mouse anti-Syt1, anti-mouse-AF647). (C and D) Labelling of postsynapses using both GluA and GluN antibodies (mouse anti-GluA, anti-mouse-AF647; rabbit anti-GluN, anti-rabbit-AF647). (A and C) Ion beam (IB)-induced secondary electron images of plunge-frozen neurons. The cell body and a few prominent processes can be observed (outlined by white dotted lines). Boxes indicate the regions shown in B and D, respectively. (B and D) Overlay of fluorescence signal recorded prior to milling with the IB-induced secondary electron image, indicating synapse-rich regions near the cell body that were targeted for cryo-FIB milling.

(E and F) Fluorescence images acquired at different stages of cryo-FIB milling (600 nm, 300 nm and 150 nm lamella thickness). Images show overlays of the fluorescence and reflection channels. While the presynaptic Syt1 signal was observable all the way through thin lamellae (E), the postsynaptic GluA and GluN signal was generally absent in fine lamellae (F). (G) Cryo-correlative microscopy workflow for single-color synapse targeting. Briefly, a fluorescence image collected on 150 nm- or 300 nm- thick lamellae is superimposed on a low-magnification TEM overview using 3-point registration affine transformation implemented in the MAPS software (Thermo Fisher Scientific). Regions selected on the overlay image in MAPS are located on the same TEM overview within SerialEM[S1], which is then used to collect tomographic tilt series at those locations. For further details see Figure 3 and Materials and Methods.

(H and I) Success rate of synapse targeting of the Syt1 (H) and GluA + GluN (I) labelling strategies. Success rate was defined as 100x the number of synaptic tomograms divided by the total number of tomograms recorded at fluorescent puncta. The number of tomograms per category is indicated on top of the respective bars. The categories were defined as follows: “synapse” refers to tomograms with clear synaptic contacts, containing a presynaptic terminal with SVs tethered at the AZ, and a postsynaptic partner separated by a well-defined synaptic cleft; “putative synapse” indicates cases where the synaptic contact was not as clear, e.g. due to missing wedge artifacts; “others” refers to non-synaptic areas.

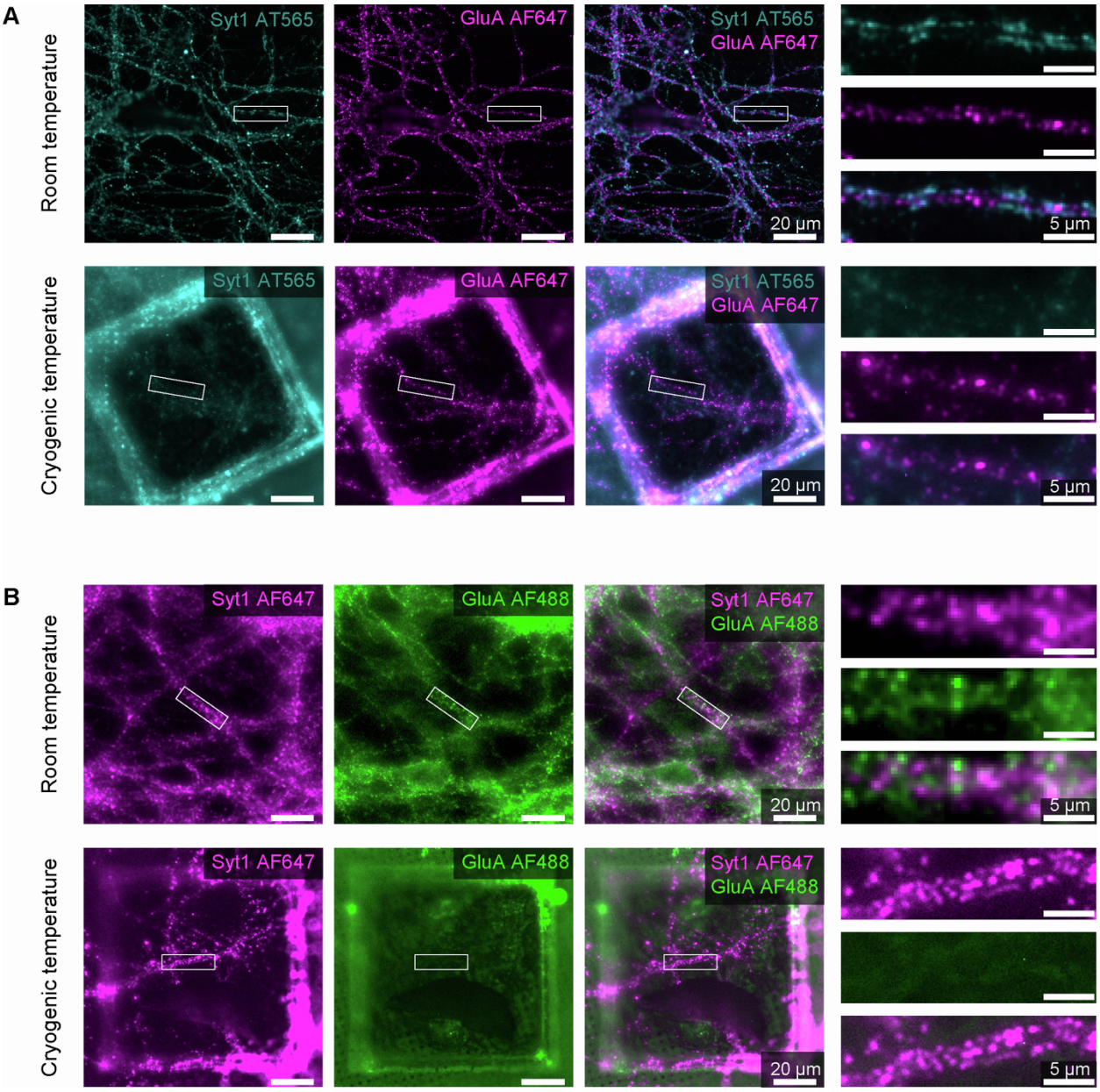

Figure S4. Live dual labelling of synapses at room temperature and under cryogenic conditions, related to Figure 1.

(A) Neuronal cultures labelled with antibodies against presynaptic Syt1 (luminal domain) conjugated with ATTO565 (cyan) and postsynaptic GluA with AF647 (magenta). Magnified views of a neuronal process are shown on the right. At room temperature (top row), fluorescence was observed for both targets, whereas under cryogenic conditions (bottom row), only AF647 signal was detected. Images at room temperature were taken after fixation and mounting of the coverslip, whereas images at cryogenic temperature were taken after vitrification of the grid. (B) Neuronal cultures labelled with antibodies against presynaptic Syt1 (luminal domain) conjugated with AF647 (magenta) and postsynaptic GluA with AF488 (green). Magnified views of a neuronal process are shown on the right. At room temperature (top row), fluorescence was observed for both targets, whereas under cryogenic conditions (bottom row), only AF647 signal was detected. Images at room temperature were taken after fixation of cells grown on the glass bottom of a Petri dish, whereas images at cryogenic temperature were taken after vitrification of the grid. See also Table S1.

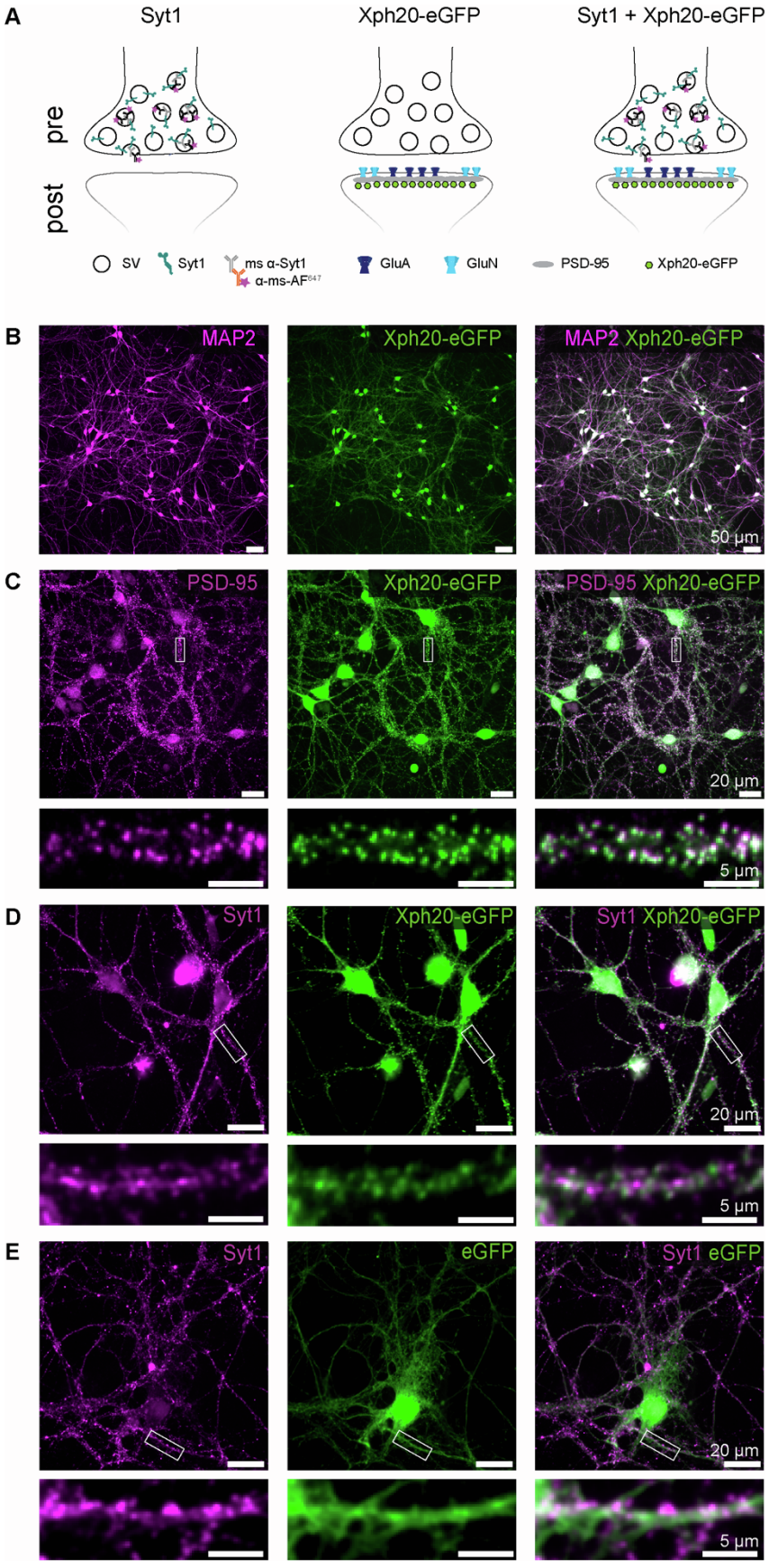
A
Syt1
Xph20-eGFP
Syt1 + Xph20-eGFP
pre
post
SV
Syt1
ms α-Syt1
α-ms-AF647
GluA
GluN
PSD-95
Xph20-eGFP
B
MAP2
Xph20-eGFP
MAP2 Xph20-eGFP
50 µm
C
PSD-95
Xph20-eGFP
PSD-95 Xph20-eGFP
20 µm
5 µm
D
Syt1
Xph20-eGFP
Syt1 Xph20-eGFP
20 µm
5 µm
E
Syt1
eGFP
Syt1 eGFP
20 µm
5 µm

Figure S5. Synthetic PSD-95 binder Xph20-eGFP as a postsynaptic marker for synaptic targeting, related to Figure 2.

(A) Schematic of the labelling strategy: Syt1 luminal domain antibody marks presynapses (left), Xph20-eGFP binds to postsynaptic PSD-95 (middle), and the combination of both markers is used to label synapses (right). pre: presynaptic terminal; post: postsynaptic terminal.

(B) Neuron-specific expression of Xph20-eGFP. Primary hippocampal neurons were transduced with AAV-Xph20-eGFP (green), fixed and immunostained with an antibody against the pan-neuronal marker MAP2 (magenta). All cells positive for Xph20-eGFP were also positive for MAP2 (white), indicating that the construct was exclusively expressed in neurons. (C) Xph20-eGFP binds to endogenous PSD-95. Neurons transduced with AAV-Xph20-eGFP (green) were immunolabelled with anti-PSD-95 to visualize endogenous PSD-95 (magenta). Insets are magnified from boxed regions in the respective images. Xph20-eGFP signal co-localized with endogenous PSD-95, showing that the construct efficiently labels postsynapses. (D and E) Xph20-eGFP-positive terminals co-localized with Syt1. Neurons were fixed upon live Syt1 labelling (mouse anti-Syt1, anti-mouse-AF647) and AAV transduction with Xph20-eGFP (D) or eGFP (E). In contrast to the diffuse signal of eGFP, Xph20-eGFP showed punctuated signals co-localizing with Syt1 (insets).

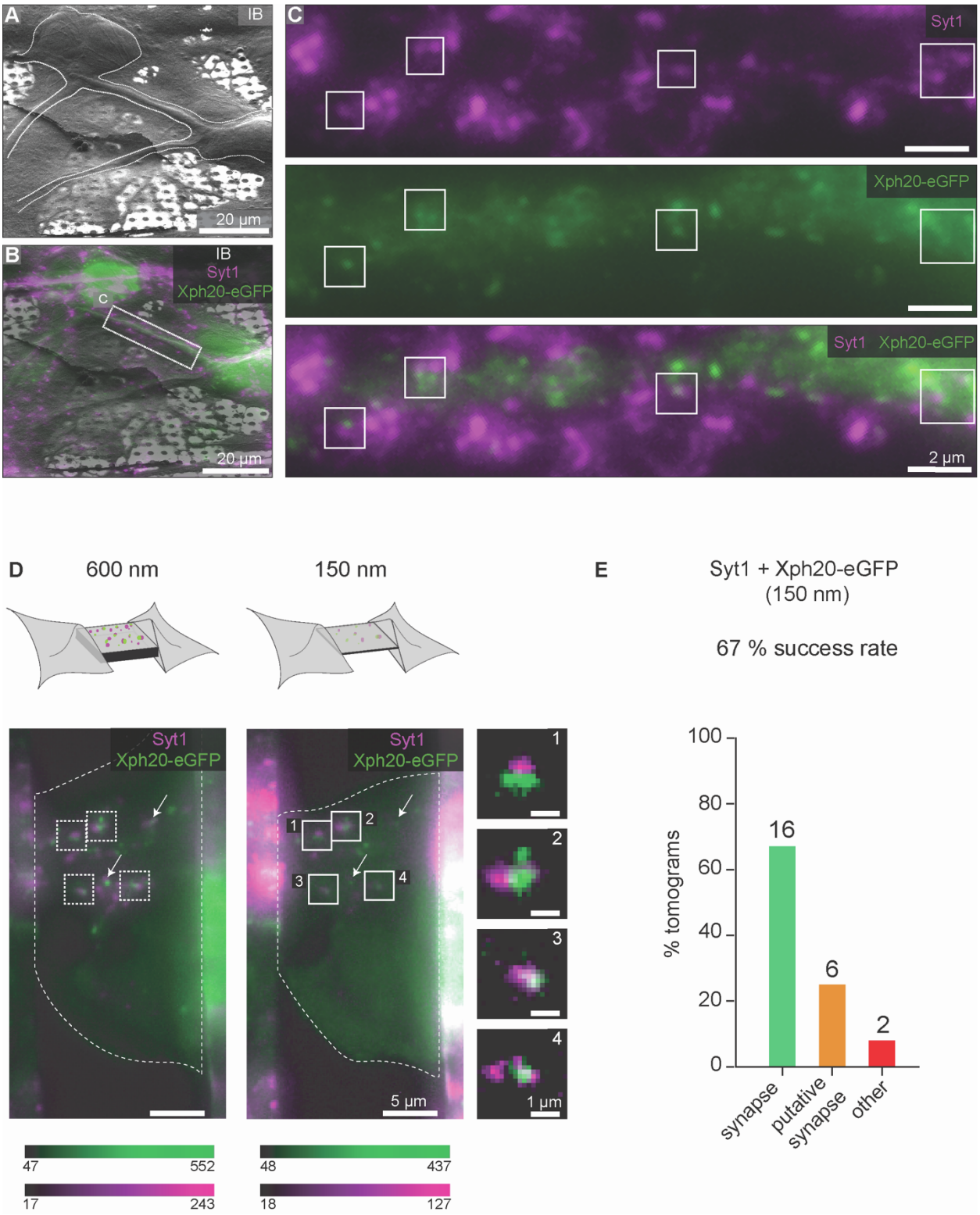

Figure S6. Cryo-FIB milling of synapses using Syt1 and Xph20-eGFP dual labelling, related to Figure 2.

(A) Ion beam (IB)-induced secondary electron image of two cultured neurons plunge-frozen on an EM grid. (B) IB-induced secondary electron image overlaid with fluorescence of Syt1 (magenta) and Xph20-eGFP

(green). A box indicates the region shown in C. (C) Magnified fluorescence images of pre- and postsynaptic signals along the neuronal process indicated in B. Boxed regions highlight co-localizations of Syt1 and Xph20-eGFP.
(D) On-lamella fluorescence acquired at different stages of cryo-FIB milling (~600 nm and ~150 nm thickness, respectively), with merged presynaptic Syt1 signal (magenta) and postsynaptic Xph20-eGFP signal (green). The dotted outlines show the shape of the lamella (visible in the green channel). The dotted boxes in the 600 nm-thick lamella mark co-localizations of pre- and postsynaptic signals. The boxed regions in the 150 nm-thick final lamella show the same areas still displaying fluorescence, corresponding to regions where cryo-tomograms can be collected. Insets (1-4) show magnified views of the co-localized puncta (insets were background subtracted to enhance contrast). For visualization purposes, the intensity of both images was scaled to approximately the same level. Calibration bars depicting the raw intensity values (in arbitrary units) are provided below the corresponding images. As the fluorescence intensity decreases during lamella preparation due to cellular material ablation, fluorescence was dimmer on the 150 nm thick lamella compared to the 600 nm stage. Some puncta visible at 600 nm thickness were lost in the final 150 nm-thick lamella (arrows).
(E) Success rate of synapse targeting of the Syt1+Xph20 labelling strategy. Success rate was defined as 100x the number of synaptic tomograms divided by the total number of tomograms recorded at fluorescent puncta. The number of tomograms per category is indicated on top of the respective bars. The categories were defined as follows: “synapse” refers to tomograms with clear synaptic contacts, containing a presynaptic terminal with SVs tethered at the AZ, and a postsynaptic partner separated by a well-defined synaptic cleft; “putative synapse” indicates cases where the synaptic contact was not as clear, e.g. due to missing wedge artifacts; “others” refers to non-synaptic areas.

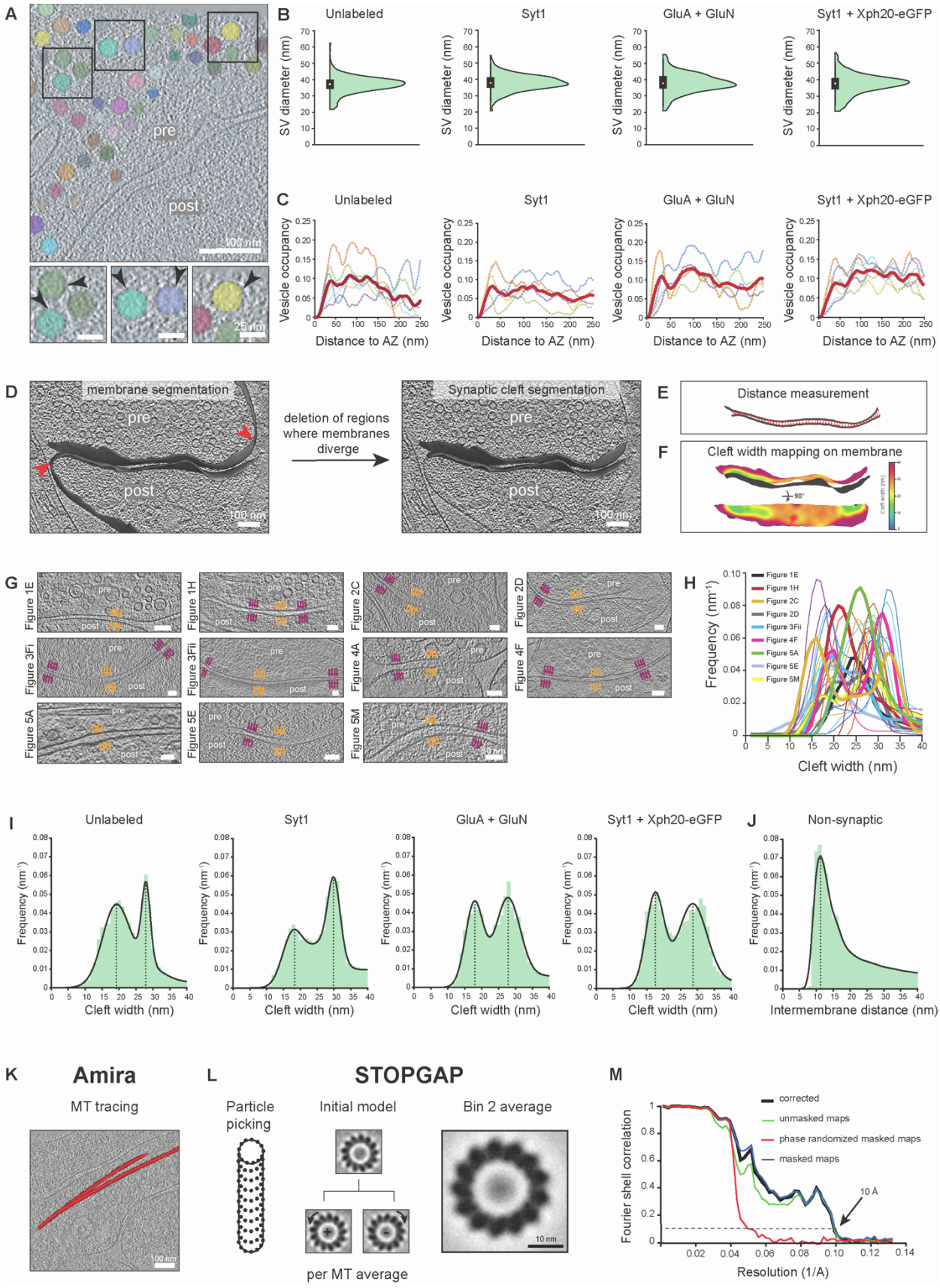
A
pre
post
100 nm
25 nm
B
Unlabeled
Syt1
GluA + GluN
Syt1 + Xph20-eGFP
SV diameter (nm)
C
Vesicle occupancy
Distance to AZ (nm)
D
membrane segmentation
pre
post
deletion of regions where membranes diverge
Synaptic cleft segmentation
E
Distance measurement
F
Cleft width mapping on membrane
90°
G
Figure 1E
Figure 1H
Figure 2C
Figure 2D
Figure 3Fi
Figure 3Fii
Figure 4A
Figure 4F
Figure 5A
Figure 5E
Figure 5M
H
Frequency (nm⁻¹)
Cleft width (nm)
I
Unlabeled
Syt1
GluA + GluN
Syt1 + Xph20-eGFP
J
Non-synaptic
Intermembrane distance (nm)
K
Amira
MT tracing
L
STOPGAP
Particle picking
Initial model
Bin 2 average
per MT average
10 nm
M
corrected
unmasked maps
phase randomized masked maps
masked maps
10 Å
Fourier shell correlation
Resolution (1/A)

Figure S7. Ultrastructural analysis of synapses and synaptic microtubule subtomogram averaging workflow, related to Figure 4 and Figure 5.

(A) SV segmentation overlaid on a tomographic slice. SVs were segmented using the SynapseNet[S2] software which delineates the SV lumen. Insets show magnified views of the boxed regions. Black arrowheads point to the SV membrane beyond the segmented SV area (shown in different colors).

(B) SV diameter measurements grouped according to the labeling strategy. Mean ± standard deviation: unlabeled, 37.0 ± 5.2 nm; Syt1, 37.8 ± 4.9 nm; GluA + GluN, 37.7 ± 5.1 nm; Syt1 + Xph20-eGFP, 37.2 ± 6.1 nm. Unlabeled, N=117; Syt1, N=382, GluA + GluN, N=289, Syt1 + Xph20-eGFP, N=287 SVs. Black boxes denote the interquartile ranges and white dots represent the median values.

(C) SV occupancy (defined as the volume fraction of presynaptic cytoplasm occupied by SVs) measurements grouped according to the labeling strategy. Dotted lines represent individual synapses and the bold line represents the mean. Unlabeled, N=6; Syt1, N=5, GluA + GluN, N=4, Syt1 + Xph20-eGFP, N=6 synapses.

(D-F) Computational workflow for synaptic cleft width measurements (see also Materials and Methods). (D) Overlay of pre and postsynaptic membrane segmentations on a tomographic slice. Red arrowheads point to regions where pre- and postsynaptic membranes begin to diverge beyond 40 nm. Membrane segmentations beyond these points were not taken into account for synaptic cleft width measurements. (E) For each point on the presynaptic membrane, the distance to its closest neighbor on the postsynaptic membrane was measured (red arrows). (F) Cleft width measurements displayed as a heatmap on the presynaptic membrane.

(G) Magnification of tomographic slices shown in the main figures centered on the synaptic cleft. Orange arrows point to the wider, central part of the cleft and purple arrows to the cleft edges.

(H-J) Intermembrane distance measurements. (H) Frequency distribution of synaptic cleft width measurements for all synapses quantitatively analyzed in this study (N=21). Traces corresponding to tomograms shown in the main figures are depicted in bold lines. The data from Figure 3Fi and Figure 4A were not included in the synaptic cleft width calculations because the membranes were severely affected by the missing wedge, resulting in incomplete segmentations. (I) Frequency distribution of synaptic cleft width measurements grouped according to the labelling strategy. The data were fit to a two-component Gaussian curve. Dotted lines mark the peak value. Mean ± standard deviation of each peak: unlabeled, 19.0 ± 6.9 nm and 28.1 ± 1.8 nm; Syt1, 18.9 ± 5.7 nm and 29.8 ± 3.9 nm; GluA + GluN, 17.6 ± 3.8 nm and 27.9 ± 5.9 nm; Syt1 + Xph20-eGFP, 17.3 ± 4.1 nm and 28.9 ± 6.5 nm. R^2 values represent the quality of the fit. Unlabeled, N=6, R^2=0.9584; Syt1, N=5, R^2=0.9104; GluA + GluN, N=4, R^2=0.9558; Syt1 + Xph20-eGFP, N=6 synapses, R^2=0.9642. (J) Frequency distribution of non-synaptic intermembrane distance measurements. As the intermembrane distances do not follow a normal dispersion, for visualization purposes a kernel distribution function was used to fit the data. The dashed line represents the peak value (11 nm). N=3 tomograms.

(K-M) Workflow for *in situ* subtomogram averaging of presynaptic microtubules (MTs). (K) Slice through a tomogram showing the tracing of presynaptic MTs represented as tubes (in red) using the Amira XFiber module (Thermo Fisher Scientific). In total, 76 MTs were traced in 18 tomograms. (L) MT averaging workflow in STOPGAP[S3]. Coordinates obtained from Amira were resampled and plotted on a tube, where each point was placed on a tubulin subunit (left). The initial reference was obtained by alignment and averaging of subtomograms extracted from one MT. All MTs (320236 subvolumes) were then aligned against this reference. Individual MT averages (middle) show the polarity of the filament. The polarity of "+" MTs was flipped and subtomograms from all MTs were aligned first at bin 4 (7.56 Å/pixel) and subsequently at bin 2 (3.78 Å/pixel). The right image shows the final bin 2 average containing 53373 subvolumes. (M) Fourier shell correlation plot of the final bin 2 average.

Presynaptic label	Postsynaptic label	Signal detected at cryogenic temperatures before cryo-FIB milling
Mouse anti-Syt1 Anti-mouse-AF647	Rabbit anti-GluN Anti-rabbit-AF488	Presynaptic
Rabbit anti-Syt1 Anti-rabbit-AF647	Mouse anti-GluA Anti-mouse-AF488	Presynaptic
Rabbit anti-Syt1 Anti-rabbit-ATTO565	Mouse anti-GluA Anti-mouse-AF647	Postsynaptic
Mouse anti-Syt1 Anti-mouse-AF647	-	Presynaptic
Rabbit anti-Syt1 Anti-rabbit-AF647	-	Presynaptic
Mouse anti-Syt1-ATTO647N	-	Presynaptic
Rabbit anti-Syt1 Anti-rabbit-ATTO565	-	-
Rabbit anti-Syt1 Anti-rabbit-AF488	-	-
-	Mouse anti-GluA Anti-mouse-AF488	-
-	Mouse anti-GluA Anti-mouse-AF647	Postsynaptic

Table S1. Strategies for immunolabelling of pre- and postsynaptic terminals at cryogenic temperatures, related to Figure 1.
All combinations displayed typical synaptic staining at room temperature (for examples, see Figure S4), but only Alexa Fluor 647 (AF647) fluorescence was observed at cryogenic temperatures prior to cryo-FIB milling, preventing dual-colour immunolabelling. The underlying reasons require further investigation, and may include insufficient labelling density, poor optics of the cryo-CLEM setups relying on low NA air objectives, and/or spectral shifts of the fluorophores at liquid nitrogen temperature.

Data collection	
Electron microscope	Titan Krios G4
Voltage (kV)	300
Camera	Falcon 4i
Collection mode	Electron counting
Nominal magnification	33000/ 42000/ 64000
Pixel size (Å/pixel)	3.65/ 2.94/ 1.89
Energy filter (eV)	20
Total exposure (e/Å^2)	120
Tilt step and range	-45°/+60°, 3° step, starting at 9°
Tilt scheme	Dose-symmetric
Defocus range (μm)	-4 to -6
Software	SerialEM

Table S2. Cryo-ET data collection table, related to STAR Methods.

Supplemental references

[S1]. Mastronarde, D.N. (2005). Automated electron microscope tomography using robust prediction of specimen movements. J. Struct. Biol. *152*, 36–51. https://doi.org/10.1016/j.jsb.2005.07.007.

[S2]. Muth, S., Moschref, F., Freckmann, L., Mutschall, S., Hojas-Garcia-Plaza, I., Bahr, J.N., Petrovic, A., Do, T.T., Schwarze, V., Archit, A., et al. (2025). SynapseNet: Deep learning for automatic synapse reconstruction. Mol. Biol. Cell *36*, ar127. https://doi.org/10.1091/mbc.E24-11-0519.

[S3]. Wan, W., Khavnekar, S., and Wagner, J. (2024). STOPGAP: an open-source package for template matching, subtomogram alignment and classification. Acta Crystallogr. Sect. Struct. Biol. *80*. https://doi.org/10.1107/S205979832400295X.